Scientia Iranica A (2012) 19 (4), 982–991

Sharif University of Technology

Scientia Iranica

Transactions A: Civil Engineering

www.sciencedirect.com

Stochastic system identification via particle and sigma-point Kalman filtering

S. Eftekhar Azam, M. Bagherinia, S. Mariani *

Politecnico di Milano, Dipartimento di Ingegneria Strutturale, Piazza L. da Vinci 32, 20133 - Milano, Italy

Received 18 May 2011; revised 6 April 2012; accepted 15 May 2012

KEYWORDS

System identification;
Nonlinear constitutive laws;
Sigma-point Kalman filtering;
Particle filtering.

Abstract In this paper, joint identification for structural systems, characterized by severe nonlinearities (softening) in the constitutive model, is pursued via the Sigma-Point Kalman Filter (S-PKF) and the Particle Filter (PF). Since a formal proof of the effects of softening in a stochastic structural system on the accuracy and stability of the filters is still missing, we comparatively assess the performances of S-PKF and PF. We show that the PF displays a higher convergence rate towards steady-state model calibrations and the S-PKF is less sensitive to the measurement noise. Both S-PKF and PF are robust, even if they tend to get unstable when a structural failure is triggered.

1. Introduction

Structural failures due to localized damaging/cracking processes can be effectively modeled through nonlinear constitutive laws featuring strength (and even elastic) degradation beyond a critical threshold, namely, through softening (see e.g. [1,2]). Accounting for the ongoing phenomena taking place inside the structure, several nonlinear models have been proposed for ductile metals [3–6], quasi-brittle ceramics and concrete-like materials [7–9], and composites [10–13]. In the last case, because of the microstructure, phenomenological models describing the whole failure event, up to structural collapse, require the tuning of a great number of constitutive parameters; this can be achieved by purposely assuming the structural state to be additional (time-varying) variables in need of filtering (actually, tracking), and approaching the problem according to joint system identification.

Simultaneous state tracking and model calibration for stochastic dynamic systems are usually obtained via the Extended Kalman Filter (EKF) [14,15]. However, in the presence of severe nonlinearities due to strength and/or stiffness degradation, the EKF may become unstable [16–18]. To preserve filter stability and converge toward steady-state estimates of model parameters, several alternative approaches have been recently proposed. Among them, the most interesting ones, from structural dynamics viewpoint, are the extended-iterated Kalman filter [14,19], the dual extended Kalman filter [20,21], and the unscented, or Sigma-Point Kalman Filter (S-PKF) [22–28]. The first two filtering techniques were shown to perform better than the EKF (see e.g. [21]), but they entail additional computational costs; hence, their use for e.g. on-line health monitoring procedures looks prevented. On the contrary, the S-PKF displays excellent performance also in highly noisy environments without increasing the computational burden [29]. A key feature of the S-PKF is that it avoids any Taylor series expansions of the evolution equations (which are nonlinear due to the degrading material properties caused by damage or crack growth), but instead introduces a deterministic sampling of the statistical distribution of the system state, and eventually allows a nonlinear evolution of each sample [22].

However, the S-PKF always assumes the initial probability density function for each state variable to be Gaussian; this assumption drives the aforementioned sampling scheme. If the joint probability density function of state variables and model parameters is not Gaussian, an approximation is obviously introduced into the solution by the S-PKF. Even if the initial distribution of the variables is Gaussian, in the case of nonlinear state-space equations the distribution itself becomes

* Corresponding author. Tel.: +39 02 23994279; fax: +39 02 23994220.
E-mail address: stefano.mariani@polimi.it (S. Mariani).

Peer review under responsibility of Sharif University of Technology.

Production and hosting by Elsevier

1026-3098 © 2012 Sharif University of Technology. Production and hosting by Elsevier B.V. Open access under CC BY-NC-ND license.
doi:10.1016/j.scient.2012.06.007

non Gaussian as the system evolves. Extensive research was carried out on the use of Gaussian filtering to develop algorithms for non Gaussian systems, but as the dimension of state of the system increases, these methodologies become computationally inefficient [30]. To assess the efficiency and accuracy of the S-PKF, here we adopt a standard particle filtering technique [31].

Aiming to develop a real-time health monitoring procedure for composite structures experiencing delamination under dynamic loadings [16,21], in this study, we focus on a single Degree-Of-Freedom (DOF) structural system. Accounting for a single DOF does not necessarily mean that the system has to be constituted by a rigid block connected to the ground via a spring and a dashpot. For instance, in [32], the authors considered a specific loading condition to excite a single vibration mode of a cantilever beam; hence, such an approach can be generally extended to resonating structures and micro-structures. The adoption of single DOF or simple systems to study the performance and stability of filters can be traced back to [33], where a linear evolution law was handled to assess the asymptotic behavior of the EKF. Nonlinear evolution laws and side constraints were then accounted for in e.g. [34,35]. Among the contributions more focused on the links between the mechanical response of the system and the solution of joint system identification problems, nonlinearities arising from post-buckling or large deflection of beam-like structures and characterizing Duffing oscillators were considered in [36–39].

In all the aforementioned studies, the mechanical response of the system was assumed to be stable: the stiffness of the spring, even when it depends on the current state, is always positive. In this paper, we instead focus on the effects on system identification of a degradation of the mechanical properties leading to a negative tangent stiffness. This case is extremely important for practical applications relevant to composites, since the nucleation and subsequent propagation of inner defects (like cracks or delamination) can eventually cause the failure of the whole structure and need to be prevented or foreseen. Since positive-definiteness of the tangent stiffness (implicitly entering the system evolution equations) and boundedness of the displacement (being part of the state variables) do not hold true in the softening regime, we investigate the links between system instability and relevant constitutive model calibration to check whether it gets affected by instability or at least error accumulation over time. We comparatively present the outcomes of S-PKF and PF; independently of the loading type and of the noise level, these two filters are expected to outperform the EKF.

We actually show that the S-PKF behaves optimally as for state tracking; even if the observed variable is diverging because of a structural failure, the whole state of the system can be accurately tracked. As far as the calibration of softening material laws is concerned, outcomes diverge or at least get biased by measurement errors in the diverging dynamics case. We also show that the PF is a very robust scheme for the investigated applications, and its convergence rate is slightly better than that of the S-PKF, even if model calibration turns out to be less accurate.

The remainder of the paper is organized as follows. In Section 2, we discuss the features of the single DOF system here investigated, highlighting the possible links with filter performance. In Section 3, we focus on filtering, specifically discussing how the probability density function is sampled by the PF and by the S-PKF. Section 4 presents a comparative discussion on state tracking and model calibration obtained with the two filters. To show the impact of nonlinearities on the results, we first study a linear system (considered as an initial benchmark), and then move to a highly nonlinear case. In Section 5, we present a discussion on the still open issues of S-PKF and PF, and then provide an overview on possible future developments. Appendix eventually reports analytical details relevant to the effects of system instability on filtering to discuss divergence causes in the presence of a spring failure.

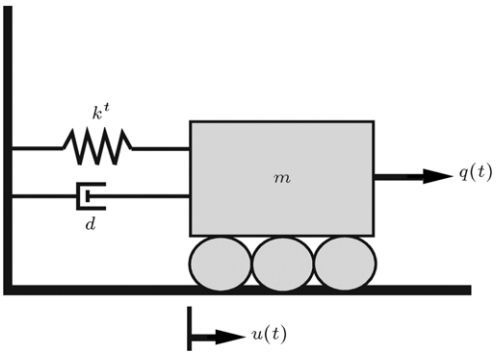

Figure 1: Single degree-of-freedom structural system.

2. Dynamic of single DOF systems

Previous studies (see e.g. [17]) showed that structural effects may have a detrimental impact on filter performance, specifically leading to poor model calibration. This happens when the sensitivity of the observed state components to constitutive parameters gets small (negligible, in principle) because of the structural dynamics. Since identifiability of nonlinear systems is still an open issue, in this work, we purposely avoid mask effects caused by the dynamics of the whole structure [17,19]. We therefore focus on a single DOF system, constituted by a mass (or rigid block) connected to the reference frame through a viscous damper and a spring (see Figure 1). The equation of motion of the system then reads:

$$m\ddot{u} + d\dot{u} + r = q, \tag{1}$$

where m is the block mass; d is the viscous damping coefficient; r is the longitudinal force in the spring; q is the external load, which may evolve in time; u, $\dot{u}$ and $\ddot{u}$ are the displacement, velocity and acceleration of the block, respectively. r can be a nonlinear function of the displacement, u; in Figure 1, k^t then represents the tangent stiffness of the spring, i.e. $k^t = \frac{\partial r}{\partial u}$ in case of holonomic responses.

To assess the performance of the filters, we account for a linear spring behavior according to:

$$r = ku, \tag{2}$$

and a highly nonlinear, RFS-type [12,40,41] spring response, governed by:

$$r = ku\exp[-nu], \tag{3}$$

where k now represents the initial stiffness of the spring, i.e. $k = k^t(u = 0)$. In Eqs. (2) and (3), k and n are (at least partially) unknown model parameters that need to be tuned in a noisy environment.

The target spring responses relevant to Eqs. (2) and (3), to be identified via the forthcoming pseudo-experimental tests, are comparatively depicted in Figure 2. Relation (2) can be used to model materials in the benchmarking elastic regime. Relation (3) can instead describe the inception and subsequent

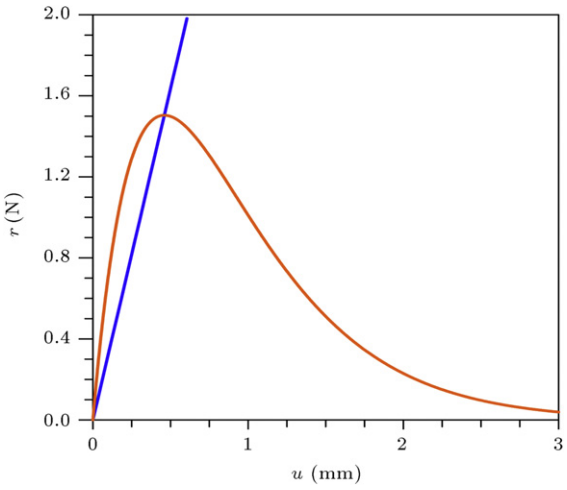

Figure 2: Linear (blue) and exponential-softening (orange) target spring responses.

growth of failure phenomena in the softening regime, beyond the force peak. In fact, damaging and cracking processes in quasi-brittle materials lead to a reduction in strength, i.e. of the load-bearing capacity. Moreover, they also cause a reduction in elastic properties. In the nonlinear constitutive model, shown in Figure 2, under tensile loading, this is captured by a decreasing slope of the unloading/reloading paths. In Section 4, we will not account for this elastic degradation process, since from the model identification viewpoint, this would require adding of relevant internal variables to the state vector (see e.g. [23]).

The two spring responses introduced above have been chosen in order to comparatively assess the outcomes of the filters, especially in terms of tuning of the constitutive laws, and to understand the impact of material nonlinearities on the results. It was already reported in [18,23] that divergence of the system (i.e. displacement of the mass unboundedly increasing in time under the applied loading), due to spring failure, may lead to unstable estimates of model parameters, diverging as well.

3. Filtering

Aiming to calibrate the constitutive model and simultaneously track the whole state of the system, we adopt an explicit Newmark integration scheme to advance the solution of Eq. (1) in the time interval, $[t_0\ t_N] \cup_{i=1}^{N_t} [t_{k-1}\ t_k]$. According to a standard predictor-integrator-corrector splitting [42], within the time step, $[t_{k-1}\ t_k]$, with $\Delta t = t_k - t_{k-1}$, the scheme reads:

- Predictor:

$$\tilde{u}_k = u_{k-1} + \Delta t \dot{u}_{k-1} + \Delta t^2 \left(\frac{1}{2} - \beta\right) \ddot{u}_{k-1}, \tag{4}$$

$$\tilde{\dot{u}}_k = \dot{u}_{k-1} + \Delta t(1-\gamma)\ddot{u}_{k-1}. \tag{5}$$

- Explicit integrator:

$$\ddot{u}_k = \frac{1}{m}[q_k - d\tilde{\dot{u}}_k - r(\tilde{u}_k)]. \tag{6}$$

- Corrector:

$$u_k = \tilde{u}_k + \Delta t^2 \beta \ddot{u}_k, \tag{7}$$

$$\dot{u}_k = \tilde{\dot{u}}_k + \Delta t \gamma \ddot{u}_k, \tag{8}$$

where $u_{k-1} = u(t_{k-1})$, $u_k = u(t_k)$ and so on. The algorithmic coefficients, β and γ, are set to $\beta = 1/4$ and $\gamma = 1/2$ (average acceleration method, see [42]).

The above Newmark time-integration scheme allows us to define the system state vector at time t_k as:

$$\mathbf{z}_k = \{u_k\ \dot{u}_k\ \ddot{u}_k\}^{\mathrm{T}}, \tag{9}$$

where $^{\mathrm{T}}$ stands for transpose. Joint identification is then obtained by introducing a so-called joint state vector, $\mathbf{x}_k$, which collects vector $\mathbf{z}_k$ and all the model parameters to be identified and gathered by vector $\boldsymbol{\vartheta}_k$:

$$\mathbf{x}_k = \{\mathbf{z}_k\ \boldsymbol{\vartheta}_k\}^{\mathrm{T}}. \tag{10}$$

In accordance with the contents of Section 2, $\boldsymbol{\vartheta}$ collects, in this study, the stiffness, k, and the further parameter, n, if the exponential law is considered.

We now assume that state $\mathbf{x}_k$ of the system, with initial (at time t_0) probability density $p(\mathbf{x}_0)$, evolves within the time step, $[t_{k-1}\ t_k]$, as a partially observed first-order Markov process, according to the conditional probability density, $p(\mathbf{x}_k|\mathbf{x}_{k-1})$. The observations, $\mathbf{y}_k$, at instant t_k are assumed to be conditionally independent, given the state, and are generated according to the conditional probability density, $p(\mathbf{y}_k|\mathbf{x}_k)$. In a noisy environment, the state-space representation of the system thus reads:

$$\begin{aligned} \mathbf{x}_k &= \mathbf{f}(\mathbf{x}_{k-1}, \mathbf{v}_{k-1}), \\ \mathbf{y}_k &= \mathbf{h}(\mathbf{x}_k, \mathbf{w}_k), \end{aligned} \tag{11}$$

where $\mathbf{v}_{k-1}$ is the process noise, and $\mathbf{w}_k$ is the observation or measurement noise. The state transition density, $p(\mathbf{x}_k|\mathbf{x}_{k-1})$, is fully specified by the mapping, $\mathbf{f}$, and by the process noise distribution, $p(\mathbf{v}_k)$, whereas $\mathbf{h}$ and observation noise distribution $p(\mathbf{w}_k)$ fully drive the observation likelihood, $p(\mathbf{y}_k|\mathbf{x}_k)$. Details on mapping $\mathbf{f}$, relevant to the current formulation and accounting for the spring responses in Eqs. (2) and (3), are reported in Appendix.

In a Bayesian framework, the posterior density, $p(\mathbf{x}_k|\mathbf{y}_{1:k})$, of the state, given all observations $\mathbf{y}_{1:k} = \{\mathbf{y}_1, \mathbf{y}_2, \ldots, \mathbf{y}_k\}$, represents the complete solution to the sequential probabilistic inference problem. Any optimal estimate of the state, such as the conditional mean, $\hat{\mathbf{x}} = \mathbb{E}[\mathbf{x}_k|\mathbf{y}_{1:k}] = \int \mathbf{x}_k p(\mathbf{x}_k|\mathbf{y}_{1:k}) d\mathbf{x}_k$, can then be computed.

By making use of the Bayes rule and the dynamic state-space model of the system, the recursive update of the posterior density becomes [43]:

$$\begin{aligned} p(\mathbf{x}_k|\mathbf{y}_{1:k}) = \frac{p(\mathbf{y}_k|\mathbf{x}_k)p(\mathbf{x}_k|\mathbf{y}_{1:k-1})}{p(\mathbf{y}_k|\mathbf{y}_{1:k-1})} &= \frac{1}{p(\mathbf{y}_k|\mathbf{y}_{1:k-1})} \\ &\times \int \delta(\mathbf{y}_k - \mathbf{h}(\mathbf{x}_k, \mathbf{w}_k)) p(\mathbf{v}_k) d\mathbf{v}_k \\ &\times \int p(\mathbf{x}_k|\mathbf{x}_{k-1}) p(\mathbf{x}_{k-1}|\mathbf{y}_{1:k-1}) d\mathbf{x}_{k-1}, \end{aligned} \tag{12}$$

where $\delta(\cdot)$ denotes the Dirac delta function. The multi-dimensional integrals in Eq. (12) are usually tractable for linear Gaussian systems only. In this case, the closed-form solution is given by the Kalman filter [44]. For nonlinear and/or non-Gaussian systems, approximate solutions must be adopted to compute the multi-dimensional integrals.

In what follows, to slightly simplify the problem and to actually account for standard test set-ups, we assume a linear relationship between observables $\mathbf{y}_k$ and state vector $\mathbf{x}_k$, governed by matrix $\mathbf{H}$ instead of mapping $\mathbf{h}$ (see [23]). If the

measured variable is the displacement or the velocity of the mass, **H** turns out to be a Boolean matrix. Moreover, noises in Relations (11) are considered to be additive, uncorrelated white and Gaussian processes, with zero mean and time-invariant covariances, **V** and **W** [14,20].

3.1. Particle filtering

Sequential Monte-Carlo methods make no explicit assumptions concerning the form of the posterior density, $p(\mathbf{x}_k|\mathbf{y}_{1:k})$. These methods approximate the Bayesian integrals in Eq. (12) through finite sums, adopting a sequential importance sampling on an adaptive stochastic grid. Within this frame, the PF implements an optimal recursive Bayesian estimation by recursively approximating the complete posterior state density. A set of N_P particles, $\mathbf{x}_k^{(i)}$, drawn from the posterior distribution, $p(\mathbf{x}_k|\mathbf{y}_{1:k})$, is used to map integrals according to:

$$p(\mathbf{x}_k|\mathbf{y}_{1:k}) \approx \sum_{i=1}^{N_P} \omega_k^{(i)} \delta(\mathbf{x}_k - \mathbf{x}_k^{(i)}), \tag{13}$$

where $\omega_k^{(i)}$ is the weight associated to particle $\mathbf{x}_k^{(i)}$ at time t_k; such weight defines the importance of particle $\mathbf{x}_k^{(i)}$ in approximating the posterior probability distribution of the state of the system. Consequently, any expectations of the form $\mathbb{E}[g(\mathbf{x}_k)] = \int g(\mathbf{x}_k)p(\mathbf{x}_k|\mathbf{y}_{1:k})d\mathbf{x}_k$, g being any given function, can be approximated through $\mathbb{E}[g(\mathbf{x}_k)] \approx \sum_{i=1}^{N_P} \omega_k^{(i)} g(\mathbf{x}_k^{(i)})$.

Since it is often impossible to sample particles $\mathbf{x}_k^{(i)}$ directly from the unknown posterior density function, we make use of importance sampling from a known, easy-to-sample, proposal distribution, $\pi(\mathbf{x}_k|\mathbf{y}_{1:k})$. Under the assumptions that the states correspond to a Markov process, and that the observations are conditionally independent given the states, a recursive estimate for the weights is derived as follows:

$$\omega_k^{(i)} = \omega_{k-1}^{(i)} \frac{p(\mathbf{y}_k|\mathbf{x}_k^{(i)})p(\mathbf{x}_k|\mathbf{x}_{k-1}^{(i)})}{\pi(\mathbf{x}_k|\mathbf{x}_{k-1}^{(i)}, \mathbf{y}_{1:k})}, \tag{14}$$

where an appropriate choice of the proposal distribution, $\pi(\mathbf{x}_k|\mathbf{x}_{k-1}^{(i)}, \mathbf{y}_{1:k})$, needs to be given.

In [31], it was shown that the proposal distribution, $\pi(\mathbf{x}_k|\mathbf{x}_{k-1}, \mathbf{y}_k)$, minimizes the variance of the importance weights, conditional on $\mathbf{x}_{k-1}$ and $\mathbf{y}_k$. Nonetheless, distribution $p(\mathbf{x}_k|\mathbf{x}_{k-1})$, i.e. the transition prior, is the most popular choice for the proposal distribution. In this paper, it has been assumed to be a Gaussian probability density function, featuring **V** as the covariance matrix. Once particles are generated through sampling from the aforementioned probability density function, they are assigned the relevant importance weights. Although this procedure results in a Monte-Carlo variation higher than that obtained using the optimal proposal, $\pi(\mathbf{x}_k|\mathbf{x}_{k-1}, \mathbf{y}_k)$, the importance weights are easily updated by simply evaluating the observation likelihood density, $p(\mathbf{y}_k|\mathbf{x}_k)$, for the sampled particle set, through:

$$\omega_k^{(i)} = \omega_{k-1}^{(i)} p(\mathbf{y}_k|\mathbf{x}_k^{(i)}). \tag{15}$$

The variance of these importance weights increases stochastically over time [31]. After a few time steps, one of the normalized importance weights tends to one, while the remaining weights tend to zero. To address this rapid degeneracy, a resampling stage may be applied to the ensemble of particles to duplicate those with higher probability and discard those with lower probability. This approach allows the filter to condense the cloud of particles around the peak probability zone(s). The adopted PF is summarized in Table 1.

Table 1: Particle filter.

- Initialization at t_0:
  $\hat{\mathbf{x}}_0 = \mathbb{E}[\mathbf{x}_0]$,
  $\mathbf{x}_0^{(i)} = \hat{\mathbf{x}}_0 \quad i = 1, \ldots, N_P$,
  $\omega_0^{(i)} = p(\mathbf{y}_0|\mathbf{x}_0)$.
- At t_k for $k = 1, \ldots, N_t$
(1) Draw particles:
  $\mathbf{x}_k^{(i)} \sim p(\hat{\mathbf{x}}_k|\mathbf{x}_{k-1}^{(i)}) \quad i = 1, \ldots, N_P$.
(2) Evolve weights:
  $\omega_k^{(i)} = \omega_{k-1}^{(i)} p(\mathbf{y}_k|\mathbf{x}_k^{(i)}) \quad i = 1, \ldots, N_P$.
(3) Resample according to algorithm 2 in [45].
(4) Compute expected value:
  $\hat{\mathbf{x}}_k = \sum_{i=1}^{N_P} \omega_k^{(i)} \mathbf{x}_k^{(i)}$.

Within this frame, it is known that the estimation of (time-invariant) model parameters leads to sample impoverishment [45,46]. We then follow here the suggestion of [47] (see also [46]) and consider model parameters to be algorithmically time-varying state variables characterized by their own covariance matrix and by a relevant process noise in the evolution equations.

3.2. Sigma-point Kalman filtering

Similarly to particle filtering, the S-PKF introduces a transformation for the statistics based on a sampling scheme. The sampled values, $\mathbf{x}_{k-1}^{(i)}$, are now called sigma-points; they obviously evolve within the time step according to the fully nonlinear system dynamics, and allow the posterior distribution to be computed via a weighted sum [30]. Even if the sampling procedure much resembles that of the PF, sigma-points are deterministically deployed around the current expected state (see [22]) so as to maximize the accuracy with a small set of trials. The aforementioned deterministic drawing of the sigma-points is characterized by stationary values of the relevant weights, and by a spreading over the state space governed by the current covariance matrix, $\mathbf{P}_{k-1}$. In [30], an explanation on how integrals like those appearing in Eq. (12) are handled by the S-PKF is provided within the frame of Gaussian filtering.

The S-PKF [22,29,48,49] is detailed in Table 2. Here, $\chi^{(i)}$ and $\chi^{\star(i)}$ are the weights adopted in the merging stage at the end of the time step to build the mean and covariance of the current state (subscript $_k$ is here dropped due to the time-invariance of the weights).

To avoid an excessive spreading of samples around the current mean, $\hat{\mathbf{x}}_{k-1}$ [22], we adopt the so-called scaled unscented transformation [25,50]. The $N_{SP}+1$ sigma-points are symmetrically deployed around $\hat{\mathbf{x}}_{k-1}$ according to (see Table 2):

$$\begin{aligned} &\mathbf{\Delta}x_{k-1}^{(0)} = \mathbf{0}, \\ &\mathbf{\Delta}x_{k-1}^{(i)} = \pm\psi\sqrt{\mathbf{P}_{k-1}}\mathbf{1}^{(i)} \quad i = 1, \ldots, N_{SP}, \end{aligned} \tag{16}$$

where ψ is a scaling parameter, and $\mathbf{1}^{(i)}$ is the i-th unit vector in the state space.

To enhance the filter performance, the scaling coefficient, ψ, needs to be carefully tuned [22,25]. In [25], an upper bound on ψ at time t_0 was provided on the basis of available bounds on model parameters (if any). Anyhow, a way to optimally set its value has not yet been devised.

According to the theoretical frames discussed, e.g. in [51–53], both PF and S-PKF are expected to work properly in the

Table 2: Sigma-point Kalman filter.

• Initialization at t_0:

$$\hat{\mathbf{x}}_0 = \mathbb{E}[\mathbf{x}_0],$$
$$\mathbf{P}_0 = \mathbb{E}[(\mathbf{x}_0 - \hat{\mathbf{x}}_0)\,(\mathbf{x}_0 - \hat{\mathbf{x}}_0)^{\mathrm{T}}],$$

• At t_k, for $k = 1, \ldots, N_t$.

(1) Predictor phase:

$$\mathbf{x}_{k-1}^{(i)} = \hat{\mathbf{x}}_{k-1} + \boldsymbol{\Delta}\boldsymbol{\chi}_{k-1}^{(i)} \quad i = 0, \ldots, N_{\mathrm{SP}},$$
$$\mathbf{x}_k^{(i)} = \mathbf{f}(\mathbf{x}_{k-1}^{(i)}),$$
$$\hat{\mathbf{x}}_k^- = \sum_{i=0}^{N_{\mathrm{SP}}} \chi^{(i)} \mathbf{x}_k^{(i)},$$
$$\mathbf{P}_k^- = \mathbf{R}_k^- + \mathbf{V},$$

where:

$$\mathbf{R}_k^- = \sum_{i=0}^{N_{\mathrm{SP}}} \chi^{*(i)} (\mathbf{x}_k^{(i)} - \hat{\mathbf{x}}_k^-)\,(\mathbf{x}_k^{(i)} - \hat{\mathbf{x}}_k^-)^{\mathrm{T}}.$$

(2) Corrector phase:

$$\hat{\mathbf{x}}_k = \hat{\mathbf{x}}_k^- + \mathbf{G}_k^U (\mathbf{y}_k - \mathbf{H}\hat{\mathbf{x}}_k^-),$$
$$\mathbf{P}_k = \mathbf{P}_k^- - \mathbf{G}_k^U \mathbf{H}\mathbf{R}_k^-,$$

where

$$\mathbf{G}_k^U = \mathbf{R}_k^- \mathbf{H}^{\mathrm{T}} (\mathbf{H}\mathbf{R}_k^- \mathbf{H}^{\mathrm{T}} + \mathbf{W})^{-1},$$

linear case. Instead, in the softening regime, some of the basic assumptions in the aforementioned proofs do not hold true, and model parameter estimates can get biased. To provide a thorough explanation of the links between softening and filter performance, an analysis is reported in Appendix.

4. Results

Results here presented are related to, so-called, pseudo-experimental tests. In the absence of real experimental data concerning the dynamics of the structural system, pseudo-experimental tests consist of running (direct) analyses based on the known or target values of model parameters, and then adding a white noise of assigned variance to the outcomes. This numerical procedure allows scattered measurements to be obtained and used to feed the filters.

In all the simulations, the applied load, q (see Eq. (1)), has been assumed to monotonically grow in time according to:

$$q = 0.5 + 0.0075t \quad \text{(N)}, \tag{17}$$

(see also [18]). Since the mass is initially at rest, this increasing loading allows the nonlinear system (see Figure 2) to be stable up to $t \approx 150$ s; beyond this threshold, spring fails (i.e. the transmitted force vanishes), and the displacement, u, tends to diverge (i.e. the mass almost freely flies-off). The estimates provided by the filters may therefore be affected by the diverging displacement, and hence by the impoverishment of the information brought by measurements.

In the analyses, damping has been disregarded (i.e. $d = 0$, see Eq. (1)), while mass has been assumed as $m = 9.72\ \mathrm{Ns}^2/\mathrm{mm}$ (see [18]). Measurements are assumed to consist of the current mass displacement only. Two levels of measurement noise have been considered: a low-noise level, characterized by a standard deviation of the scattered measured displacements, $w = 0.01$ mm ($W = 10^{-4}\ \mathrm{mm}^2$), and a high-noise level characterized instead by $w = 0.05$ mm ($W = 2.5 \cdot 10^{-3}\ \mathrm{mm}^2$). Because of the initial conditions, in the simulations we have adopted $\hat{\mathbf{z}}_0 = \{0\ 0\ \frac{q_0}{m}\}^{\mathrm{T}}$. Dealing with pseudo-experimental tests, the system evolution equations can be assumed affected by small errors (see also [34]). On the basis of the a-priori knowledge about model parameter values, we have considered entries in $\hat{\boldsymbol{\vartheta}}_0$ to vary in the range between 50% and 150% of the target values; accordingly, entries of $\mathbf{P}_0$ (as for the S-PKF), assumed to be diagonal, or properties of the initial statistical distributions $p(\mathbf{x}_0)$ (as for the PF), assumed to be uncorrelated, have been set to allow convergence toward target parameter values. To speed-up the convergence of the unobservable parameter(s) in the stable dynamic regime, the relevant variances have been then increased (typically by a factor 100; see [54]). As far as PF is concerned, we have run the analyses adopting $N_{\mathrm{P}} = 500$ particles in all cases. While this turns out to be excessively time consuming in the linear case (where a set smaller by an order of magnitude can be enough to provide accurate results; see e.g. [39]), it becomes mandatory in the softening case to guarantee the same level of accuracy of the S-PKF prior to divergence.

Starting with the linear system, results relevant to the tracking of the whole state (i.e. of u, $\dot{u}$ and $\ddot{u}$) are reported in Figures 3 and 4, respectively, referring to the low- and high-noise cases. In all the plots, the dashed line represents the target system response, the orange squared symbols are the discrete-time estimations furnished by the filters, and the blue circular symbols stand for the measurements (that, we recall, consist of displacement values only). By comparing the performances of the two filters, the plots prove that both S-PKF and PF correctly capture the actual dynamics of the system independently of the noise level. A closer look at the results, anyhow, shows that the S-PKF provides a slightly more accurate tracking, since scattering of estimates around the target response is almost negligible.

Spring model calibration, shown in Figure 5 for the two considered noise levels, once again proves that the S-PKF is slightly more accurate than the PF. While both filters lead to unbiased, almost-stationary estimates of the spring stiffness, k, long-term oscillations are much smaller in magnitude if the S-PKF is adopted. None of the two filters provides biased estimates due to accumulation of errors over time. Looking at the short-term variation of the estimates, it appears instead that the PF shows a superior convergence rate towards the target value of k, even though the aforementioned oscillations set in and reduce the overall accuracy.

Moving now to the nonlinear system, Figure 6 depicts the performances of the two filters in terms of state tracking, in the high-noise environment. Both S-PKF and PF accurately track state evolution, even in the unstable regime (beyond $t \approx 150$ s) characterized by a diverging u after spring failure. As in the linear case, S-PKF provides more accurate outcomes, perfectly matching system dynamics.

An intriguing feature of the nonlinear case, related to model calibration (i.e. to the identification of k and n in Eq. (3)), is shown in Figure 7. Estimates rapidly converge to the target values, independently of the initialization guess. Stable oscillations around the targets, like those shown in the linear case, are still present, especially when the PF is adopted. As soon as the system stability threshold is approached, wild oscillations of increasing amplitude set in, eventually leading to biased (or even diverging) model calibration. For one of the initializations adopted in Figure 7, the behavior of the PF is depicted in Figure 8 in terms of current values of the importance weights, $\omega_k^{(i)}$, of all the particles, before resampling. For ease of presentation, results are reported with projections onto k and n parameter axes independently, even though they are linked to a single set of particles. Before divergence, the values of the weights are almost always higher in a region around (and close to) the target parameters. Once divergence is triggered, the filter is not able to provide higher importance to particles close to the target, and the distribution of the weights along k and n axes gets flat.

The aforementioned response of both filters cannot be obviously caused by the increased variances adopted in $\mathbf{P}_0$ and

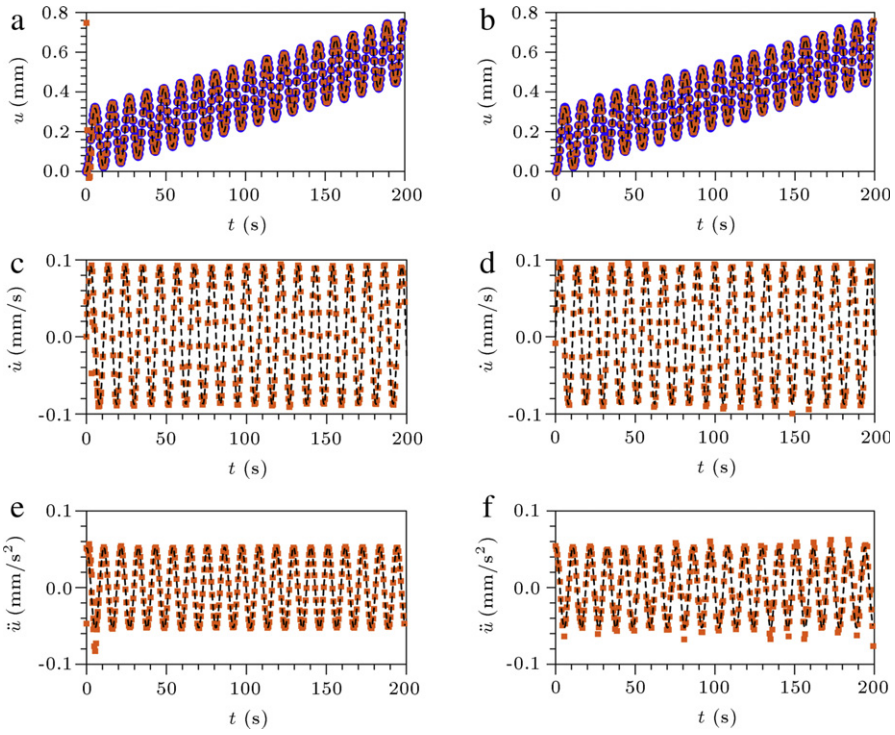

Figure 3: Linear spring model, low-noise case. Comparison between target (dashed lines) and tracked (orange squared symbols) system responses in terms of (top row) displacement u, (middle row) velocity $\dot{u}$, and (bottom row) acceleration $\ddot{u}$. Results obtained using (left column) S-PKF, and (right column) PF.

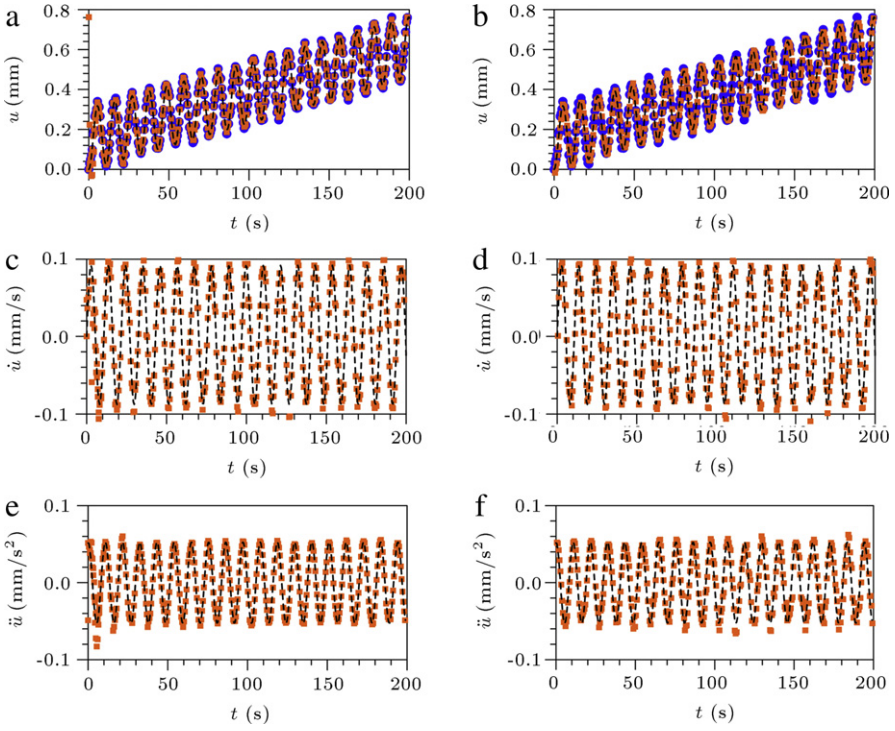

Figure 4: Linear spring model, high-noise case. Comparison between target (dashed lines) and tracked (orange squared symbols) system responses in terms of (top row) displacement u, (middle row) velocity $\dot{u}$, and (bottom row) acceleration $\ddot{u}$. Results obtained using (left column) S-PKF, and (right column) PF.

$p(\mathbf{x}_0)$ for model parameters. As said, upscaling is adopted only to speed-up the convergence toward the target values, which actually takes place in the stable regime of system dynamics. In this case, divergence is therefore due to softening.

Hence, in the softening regime accurate tracking of the partially observed state does not guarantee that unbiased estimates of model parameters, which cannot be observed at all, can be obtained with the two filters.

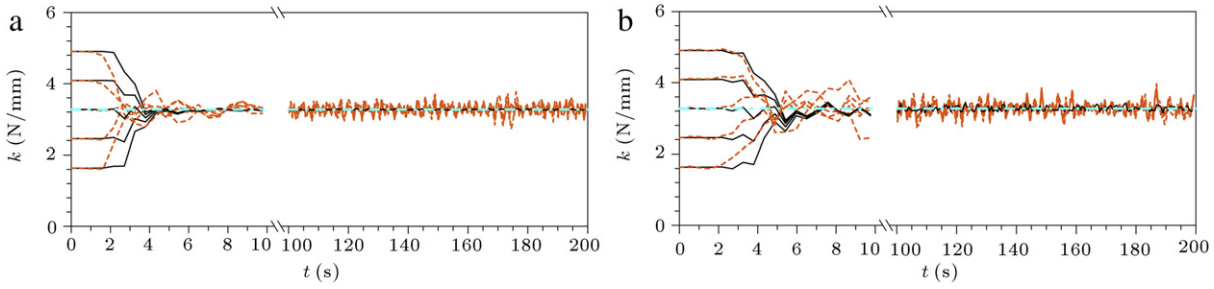

Figure 5: Linear spring model (target $\bar{k} = 3.27$ N/mm [18]). Comparison between time evolutions of the estimated spring stiffness k at varying initialization values provided by S-PKF (continuous black lines) and PF (dashed orange lines). (a) Low-noise case; and (b) high-noise case.

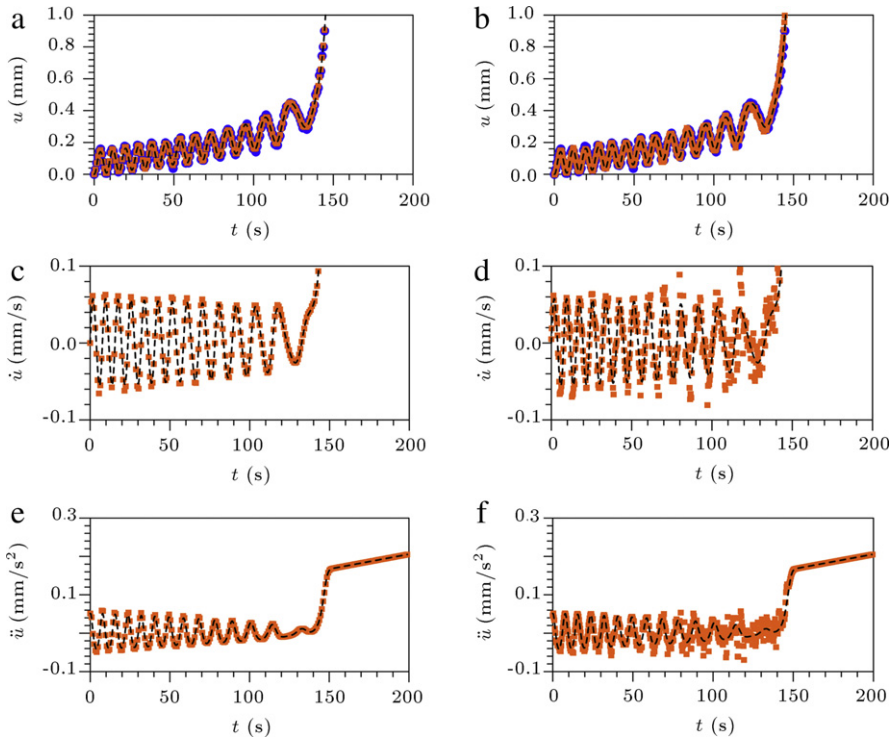

Figure 6: Exponential-softening spring model, high-noise case. Comparison between target (dashed lines) and tracked (orange squared symbols) system responses in terms of (top row) displacement u, (middle row) velocity $\dot{u}$, (bottom row) and acceleration $\ddot{u}$. Results obtained using (left column) S-PKF, and (right column) PF.

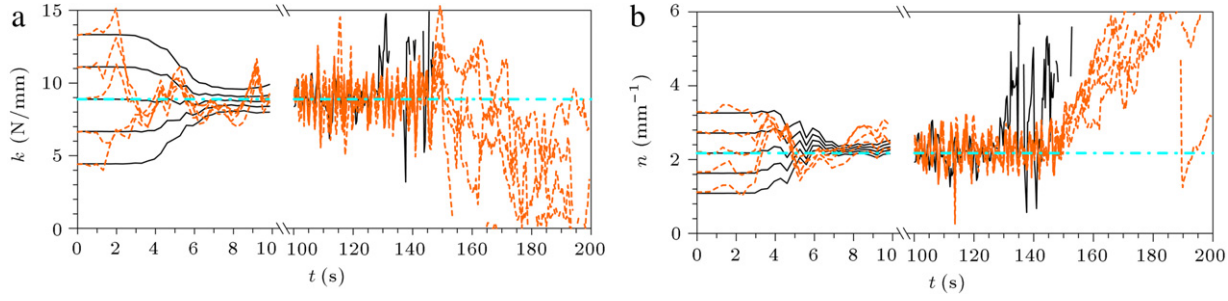

Figure 7: Exponential-softening spring model (target $\bar{k} = 8.8888$ N/mm, $\bar{n} = 2.1739$ mm^{-1} [18]), high-noise case. Comparison between time evolutions of the estimated model parameters (a) k and (b) n at varying initialization values provided by S-PKF (continuous black lines) and PF (dashed orange lines).

5. Concluding remarks

In this paper, we have comparatively assessed the performances of the sigma-point Kalman filter and of a standard particle filter. Aiming to develop a real-time health monitoring procedure for (composite) structures experiencing damaging processes caused by external actions, these two filters look appropriate since they do not entail excessive computational costs and can be parallelized (see e.g. [55,56]). Moreover, instead of the step-by-step linearization of the system evolution equations characterizing the extended Kalman filter, they exploit the statistical distribution of the state to draw samples (realizations) that subsequently evolve in time according to the true nonlinear system dynamics.

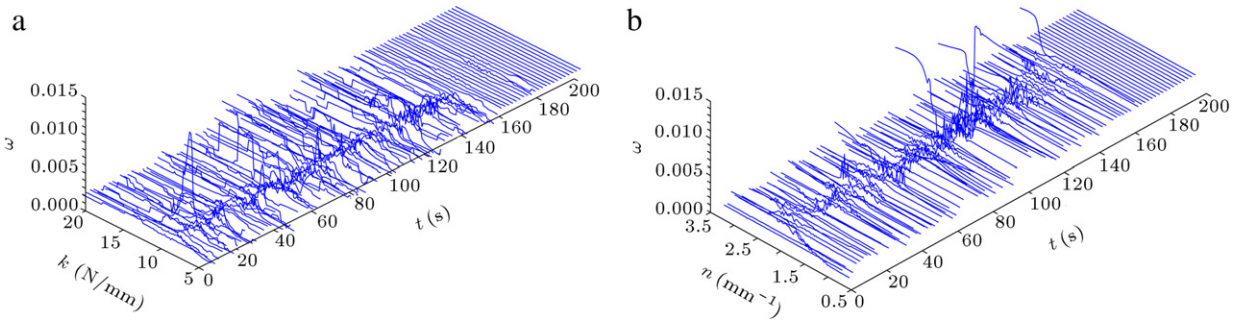

Figure 8: Exponential-softening spring model (target $\tilde{k} = 8.8888$ N/mm, $\tilde{n} = 2.1739$ mm^{-1} [18]), high-noise case. Time evolution of the importance weights $\omega_k^{(i)}$, associated to the position of particles along the (a) k and (b) n axes.

We have shown that, independently of the level of the noise affecting measurements, the filters accurately track the whole (partially observed) state. If the system behaves linearly, constitutive parameters are also perfectly tuned; if the system is instead affected by a reducing load-carrying capacity because of ongoing damaging or cracking processes, the filters efficiently provide model calibration only if displacements (i.e. observables) are not diverging. Moreover, while the PF displays a higher convergence rate towards (quasi) steady-state model parameter estimates, the S-PKF provides more accurate model calibrations independently of nonlinear effects.

Since the understanding of the effects of stability of the structural system on the performance of two filters requires additional investigations, in future work, we will provide a comparison with Monte Carlo simulations to assess the consistency and information content [57] of the estimates provided, to eventually highlight the actual reasons of fluctuating or even diverging constitutive calibrations.

Acknowledgments

This work has been developed within the frame of MIUR-PRIN08 project Mechanics of microstructured materials: multi-scale identification, optimization and active control (grant #2008KNHF9Y).

Appendix

A.1. Structural stability vs filter stability

The aim of this Appendix is to provide an explanation of why in the presence of softening we test the stability of filters or, alternatively, the convergence toward unbiased estimates of model parameters through numerical simulations, without resorting to the results of established theoretical analyses.

We first consider the S-PKF, which shares many features with EKF and also some details of the proof of stability. Specifically referring to [51,52], use is made of the Jacobian of the nonlinear evolution equations (even though it is not handled by the S-PKF). We explicitly write the state mapping $\mathbf{f}$ in Eq. $(11)_1$ as:

$$\mathbf{x}_k = \begin{Bmatrix} u_k \\ \dot{u}_k \\ \ddot{u}_k \\ \boldsymbol{\vartheta}_k \end{Bmatrix} = \mathbf{f}(\mathbf{x}_{k-1}) + \mathbf{v}_{k-1} = \begin{Bmatrix} f_u(\mathbf{x}_{k-1}) \\ f_{\dot{u}}(\mathbf{x}_{k-1}) \\ f_{\ddot{u}}(\mathbf{x}_{k-1}) \\ \boldsymbol{\vartheta}_{k-1} \end{Bmatrix} + \mathbf{v}_{k-1}, \tag{A.1}$$

where scalar functions f_u, $f_{\dot{u}}$ and $f_{\ddot{u}}$ implicitly gather Eqs. (4)–(8). As in Section 3, process noise $\mathbf{v}_{k-1}$ is assumed to be an additive term. The Jacobian of the state mapping in the exponential constitutive law case thus reads:

$$\mathbf{F}_{k-1} = \left.\frac{\partial \mathbf{f}}{\partial \mathbf{x}}\right|_{\hat{\mathbf{x}}_{k-1}} = \begin{bmatrix} \frac{\partial f_u}{\partial u_{k-1}} & \frac{\partial f_u}{\partial \dot{u}_{k-1}} & \frac{\partial f_u}{\partial \ddot{u}_{k-1}} & \frac{\partial f_u}{\partial k_{k-1}} & \frac{\partial f_u}{\partial n_{k-1}} \\ \frac{\partial f_{\dot{u}}}{\partial u_{k-1}} & \frac{\partial f_{\dot{u}}}{\partial \dot{u}_{k-1}} & \frac{\partial f_{\dot{u}}}{\partial \ddot{u}_{k-1}} & \frac{\partial f_{\dot{u}}}{\partial k_{k-1}} & \frac{\partial f_{\dot{u}}}{\partial n_{k-1}} \\ \frac{\partial f_{\ddot{u}}}{\partial u_{k-1}} & \frac{\partial f_{\ddot{u}}}{\partial \dot{u}_{k-1}} & \frac{\partial f_{\ddot{u}}}{\partial \ddot{u}_{k-1}} & \frac{\partial f_{\ddot{u}}}{\partial k_{k-1}} & \frac{\partial f_{\ddot{u}}}{\partial n_{k-1}} \\ 0 & 0 & 0 & 1 & 0 \\ 0 & 0 & 0 & 0 & 1 \end{bmatrix}, \tag{A.2}$$

where:

$$\begin{aligned}
&\frac{\partial f_u}{\partial u_{k-1}} = 1 + \beta \Delta t^2 \frac{\partial \ddot{u}_k}{\partial u_{k-1}}, \\
&\frac{\partial f_u}{\partial \dot{u}_{k-1}} = \Delta t + \beta \Delta t^2 \frac{\partial \ddot{u}_k}{\partial \dot{u}_{k-1}}, \\
&\frac{\partial f_u}{\partial \ddot{u}_{k-1}} = \left(\frac{1}{2} - \beta\right) \Delta t^2 + \beta \Delta t^2 \frac{\partial \ddot{u}_k}{\partial \ddot{u}_{k-1}}, \\
&\frac{\partial f_u}{\partial k_{k-1}} = \beta \Delta t^2 \frac{\partial \ddot{u}_k}{\partial k_{k-1}}, \\
&\frac{\partial f_u}{\partial n_{k-1}} = \beta \Delta t^2 \frac{\partial \ddot{u}_k}{\partial n_{k-1}}, \\
&\frac{\partial f_{\dot{u}}}{\partial u_{k-1}} = \gamma \Delta t \frac{\partial \ddot{u}_k}{\partial u_{k-1}}, \\
&\frac{\partial f_{\dot{u}}}{\partial \dot{u}_{k-1}} = 1 + \gamma \Delta t \frac{\partial \ddot{u}_k}{\partial \dot{u}_{k-1}}, \\
&\frac{\partial f_{\dot{u}}}{\partial \ddot{u}_{k-1}} = (1 - \gamma) \Delta t + \gamma \Delta t \frac{\partial \ddot{u}_k}{\partial \ddot{u}_{k-1}}, \\
&\frac{\partial f_{\dot{u}}}{\partial k_{k-1}} = \gamma \Delta t \frac{\partial \ddot{u}_k}{\partial k_{k-1}}, \\
&\frac{\partial f_{\dot{u}}}{\partial n_{k-1}} = \gamma \Delta t \frac{\partial \ddot{u}_k}{\partial n_{k-1}}, \\
&\frac{\partial f_{\ddot{u}}}{\partial u_{k-1}} = \frac{\partial \ddot{u}_k}{\partial u_{k-1}}, \\
&\frac{\partial f_{\ddot{u}}}{\partial \dot{u}_{k-1}} = \frac{\partial \ddot{u}_k}{\partial \dot{u}_{k-1}},
\end{aligned}$$

$$\frac{\partial f_{\ddot{u}}}{\partial \ddot{u}_{k-1}} = \frac{\partial \ddot{u}_k}{\partial \ddot{u}_{k-1}},$$
$$\frac{\partial f_{\ddot{u}}}{\partial k_{k-1}} = \frac{\partial \ddot{u}_k}{\partial k_{k-1}},$$
$$\frac{\partial f_{\ddot{u}}}{\partial n_{k-1}} = \frac{\partial \ddot{u}_k}{\partial n_{k-1}},$$

and:

$$\frac{\partial \ddot{u}_k}{\partial u_{k-1}} = \frac{1}{m}\left[-\frac{\partial r(\tilde{u}_k)}{\partial \tilde{u}_k}\right],$$
$$\frac{\partial \ddot{u}_k}{\partial \dot{u}_{k-1}} = \frac{1}{m}\left[-d - \Delta t\frac{\partial r(\tilde{u}_k)}{\partial \tilde{u}_k}\right],$$
$$\frac{\partial \ddot{u}_k}{\partial \ddot{u}_{k-1}} = \frac{1}{m}\left[-d(1-\gamma)\Delta t - \left(\frac{1}{2}-\beta\right)\Delta t^2\frac{\partial r(\tilde{u}_k)}{\partial \tilde{u}_k}\right],$$
$$\frac{\partial \ddot{u}_k}{\partial k_{k-1}} = \frac{1}{m}\left[-\frac{\partial r(\tilde{u}_k)}{\partial k_{k-1}}\right],$$
$$\frac{\partial \ddot{u}_k}{\partial n_{k-1}} = \frac{1}{m}\left[-\frac{\partial r(\tilde{u}_k)}{\partial n_{k-1}}\right].$$

Eventually, the constitutive derivatives are:

$$\frac{\partial r(\tilde{u}_k)}{\partial \tilde{u}_k} = k_{k-1}(1 - n_{k-1}\tilde{u}_k)\exp[-n_{k-1}\tilde{u}_k],$$
$$\frac{\partial r(\tilde{u}_k)}{\partial k_{k-1}} = \tilde{u}_k\exp[-n_{k-1}\tilde{u}_k],$$
$$\frac{\partial r(\tilde{u}_k)}{\partial n_{k-1}} = -k_{k-1}\tilde{u}_k^2\exp[-n_{k-1}\tilde{u}_k].$$

In the case of the linear spring model, the last row and last column of matrix $\mathbf{F}_{k-1}$ in Eq. (A.2) have to be dropped, and $n_{k-1} = 0$ needs to be adopted in all the remaining entries.

According to the preceding derivation, the determinant of the Jacobian matrix is:

$$\begin{aligned}\det(\mathbf{F}_{k-1}) = {} & \frac{\partial f_u}{\partial u_{k-1}}\frac{\partial f_{\dot{u}}}{\partial \dot{u}_{k-1}}\frac{\partial f_{\ddot{u}}}{\partial \ddot{u}_{k-1}} + \frac{\partial f_u}{\partial \dot{u}_{k-1}}\frac{\partial f_{\dot{u}}}{\partial \ddot{u}_{k-1}}\frac{\partial f_{\ddot{u}}}{\partial u_{k-1}} \\ & + \frac{\partial f_u}{\partial \ddot{u}_{k-1}}\frac{\partial f_{\dot{u}}}{\partial u_{k-1}}\frac{\partial f_{\ddot{u}}}{\partial \dot{u}_{k-1}} - \frac{\partial f_u}{\partial \ddot{u}_{k-1}}\frac{\partial f_{\dot{u}}}{\partial \dot{u}_{k-1}}\frac{\partial f_{\ddot{u}}}{\partial u_{k-1}} \\ & - \frac{\partial f_u}{\partial u_{k-1}}\frac{\partial f_{\dot{u}}}{\partial \ddot{u}_{k-1}}\frac{\partial f_{\ddot{u}}}{\partial \dot{u}_{k-1}} - \frac{\partial f_u}{\partial \dot{u}_{k-1}}\frac{\partial f_{\dot{u}}}{\partial u_{k-1}}\frac{\partial f_{\ddot{u}}}{\partial \ddot{u}_{k-1}}. \end{aligned} \quad \text{(A.3)}$$

In [51,52], necessary conditions to assure the stability of filtering are the positive-definiteness and the boundedness of $\mathbf{F}_{k-1}$. In case of softening, the tangent stiffness, $\frac{\partial r(\tilde{u}_k)}{\partial \tilde{u}_k}$, of the spring becomes negative (meaning that the longitudinal force inside the spring is decreasing when the elongation is increasing), and this affects terms of $\mathbf{F}_{k-1}$ so that the Jacobian may lose positive-definiteness. Moreover, since the system becomes unstable and displacement diverges once softening is incepted (we recall that from a structural mechanics viewpoint this means that the system is failing), entries of $\mathbf{F}_{k-1}$ grow in time. This growth detrimentally affects the error performance of the S-PKF [52]. Such phenomenon can explain the fluctuations in the estimates of (unobserved) model parameters, which do not show up in the linear case and instead set in once the spring enters into the softening regime, even before system divergence.

We now move to the PF case. It was proven that PF allows, as $N_P \to \infty$, to approach the actual evolution of the statistical distribution of the state within the time step; this happens if some boundedness and positive definiteness properties of the evolution itself are met (see [53]). In the presence of softening, such conditions may not be attained, leading to the fluctuations of model parameter estimates. It is worth pointing out that the whole solution provided by the filter is not diverging, since the (partially observed) structural state is actually predicted without bias (see Section 4). Moreover, this filter response turns out to be triggered by softening, since it cannot be seen in either the linear or nonlinear cases, prior to transition to the unstable spring behavior.

References

[1] Bažant, Z.L. and Pijaudier-Cabot, G. "Nonlocal continuum damage, localization instability and convergence", *ASME Journal of Applied Mechanics*, 55, pp. 287–293 (1988).

[2] Comi, C. "A non-local model with tension and compression damage mechanisms", *European Journal of Mechanics A/Solids*, 20, pp. 1–22 (2001).

[3] Dodd, B. and Bai, Y., *Ductile Fracture and Ductility with Applications to Metalworking*, Academic Press (1987).

[4] Lemaitre, J., *A Course on Damage Mechanics*, Springer Verlag, Berlin (1996).

[5] Mariani, S. and Corigliano, A. "Anisotropic behaviour of porous-ductile media", *International Journal of Solids and Structures*, 38, pp. 2427–2451 (2001).

[6] Corigliano, A., Mariani, S. and Orsatti, B. "Identification of Gurson–Tvergaard material model parameters via Kalman filtering technique", *I. Theory, International Journal of Fracture*, 104, pp. 349–373 (2000).

[7] Jirasek, M. "Nonlocal models for damage and fracture: comparison of approaches", *International Journal of Solids and Structures*, 35, pp. 4133–4145 (1998).

[8] Jirasek, M. and Zimmerman, T. "Embedded crack model: I. Basic formulation", *International Journal for Numerical Methods in Engineering*, 50, pp. 1269–1290 (2001).

[9] Comi, C., Mariani, S. and Perego, U. "An extended FE strategy for transition from continuum damage to mode I cohesive crack propagation", *International Journal for Numerical and Analytical Methods in Geomechanics*, 31, pp. 213–238 (2007).

[10] Allix, O., Léeèveque, D. and Perret, L. "Interlaminar interface model identification and forecast of delamination in composite laminates", *Composites Science & Technology*, 58, pp. 671–678 (1998).

[11] Allix, O., Ladevéze, P. and Corigliano, A. "Damage analysis of interlaminar fracture specimens", *Composite Structures*, 31, pp. 61–74 (1995).

[12] Corigliano, A., Mariani, S. and Pandolfi, A. "Numerical analysis of rate-dependent dynamic composite delamination", *Composites Science and Technology*, 66, pp. 766–775 (2006).

[13] Ladevéze, P., Lubineau, G. and Marsal, D. "Towards a bridge between the micro- and mesomechanics of delamination for laminated composites", *Composites Science and Technology*, 66, pp. 698–712 (2006).

[14] Gelb, A., *Applied Optimal Estimation*, The M.I.T. Press, Cambridge, USA (1974).

[15] Kalman, R.E. and Bucy, R.S. "New results in linear filtering and prediction theory", *ASME Journal of Basic Engineering*, 83D, pp. 95–108 (1961).

[16] Corigliano, A. and Mariani, S. "Parameter identification of a time-dependent elasticdamage interface model for the simulation of debonding in composites", *Composites Science and Technology*, 61, pp. 191–203 (2001).

[17] Corigliano, A. and Mariani, S. "Simulation of damage in composites by means of interface models: parameter identification", *Composites Science and Technology*, 61, pp. 2299–2315 (2001).

[18] Corigliano, A. and Mariani, S. "Parameter identification in explicit structural dynamics: performance of the extended Kalman filter", *Computer Methods in Applied Mechanics and Engineering*, 193, pp. 3807–3835 (2004).

[19] Bittanti, S., Maier, G. and Nappi, A. "Inverse problems in structural elastoplasticity: a Kalman filter approach, in plasticity today", In *Modelling, Methods and Applications*, A. Sawczuk and G. Bianchi, Eds., pp. 311–329, Elsevier Applied Science Publishers, London, UK, New York, USA (1984).

[20] Wan, E. and Nelson, A., *Dual Extended Kalman Filter Methods, in Kalman Filtering and Neural Networks*, S. Haykin, Ed., pp. 123–173, John Wiley & Sons, Inc,, New York, USA (2001).

[21] Mariani, S. and Corigliano, A. "Impact induced composite delamination: state an parameter identification via joint and dual extended Kalman filters", *Computer Methods in Applied Mechanics and Engineering*, 194, pp. 5242–5272 (2005).

[22] Julier, S., Uhlmann, J. and Durrant-Whyte, H. "A new method for the nonlinear transformation of means and covariances in filters and estimators", *IEEE Transactions on Automatic Control*, 45, pp. 477–482 (2000).

[23] Mariani, S. and Ghisi, A. "Unscented Kalman filtering for nonlinear structural dynamics", *Nonlinear Dynamics*, 49, pp. 131–150 (2007).

[24] Gove, J.H. and Hollinger, D. "Application of a dual unscented Kalman filter for simultaneous state and parameter estimation in problems of surface-atmosphere exchange", *Journal of Geophysical Research*, 111, p. D08S07 (2006).
[25] Mariani, S. "Failure of layered composites subject to impacts: constitutive modeling and parameter identification issues", In *Strength of Materials*, G. Mendes and B. Lago, Eds., pp. 97–131, Nova Publishers (2009).
[26] Mariani, S. "Failure assessment of layered composites subject to impact loadings: a finite element, sigma-point Kalman filter approach", *Algorithms*, 2, pp. 808–827 (2009).
[27] Hommels, A., Murakami, A. and Nishimura, S. "A comparison of the ensemble Kalman filter with the unscented Kalman filter: application to the construction of a road embankment", *GEO International*, pp. 52–54 (2009).
[28] Mohtat, A. and Yousefi-Koma, A. "Online estimation and identification of shape memory alloy-actuated flexible structures through unscented Kalman filtering", *Journal of Intelligent Material Systems and Structures*, 21, pp. 1589–1602 (2010).
[29] Wan, E. and van der Merwe, R. "The unscented Kalman filter", In *Kalman Filtering and Neural Networks*, S. Haykin, Ed., pp. 221–280, John Wiley & Sons, Inc., New York, USA (2001).
[30] Ito, K. and Xiong, K. "Gaussian filters for nonlinear filtering problems", *IEEE Transactions on Automatic Control*, 45, pp. 910–927 (2000).
[31] Doucet, A. "Monte Carlo methods for Bayesian estimation of hidden markov models: application to radiation signals", Ph.D. Thesis, University Paris-Sud, Orsay, France (1997).
[32] Malatkar, P. and Nayfeh, A. "A parametric identification technique for single-degreeof-freedom weakly nonlinear systems with cubic nonlinearities", *Journal of Vibration and Control*, 9, pp. 317–336 (2003).
[33] Ljung, L. "Asymptotic behavior of the extended Kalman filter as a parameter estimator for linear systems", *IEEE Transactions on Automatic Control*, AC-24, pp. 36–50 (1979).
[34] Sitz, A., Schwarz, U., Kurths, J. and Voss, H. "Estimation of parameters and unobserved components for nonlinear systems from noisy time series", *Physical Review E*, 66, p. 016210 (2002).
[35] Gerdin, M., Schon, T., Glad, T., Gustafsson, F. and Ljung, L. "On parameter and state estimation for linear differential–algebraic equations", *Automatica*, 43, pp. 416–425 (2007).
[36] Jaksic, N. and Boltezar, M. "An approach to parameter identification for a singledegree-of-freedom dynamical system based on short free acceleration response", *Journal of Sound and Vibration*, 250, pp. 465–483 (2002).
[37] Ghosh, S., Manohar, C. and Roy, D. "A sequential importance sampling filter with a new proposal distribution for state and parameter estimation of nonlinear dynamical systems", *Proceedings of the Royal Society of London A: Mathematical, Physical and Engineering Sciences*, 464, pp. 25–47 (2008).
[38] Khalil, M., Sarkar, A. and Adhikari, S. "Nonlinear filters for chaotic oscillatory systems", *Nonlinear Dynamics*, 55, pp. 113–137 (2009).
[39] Khalil, M., Sarkar, A. and Adhikari, S. "Tracking noisy limit cycle oscillation with nonlinear filters", *Journal of Sound and Vibration*, 329, pp. 150–170 (2010).
[40] Rose, J., Ferrante, J. and Smith, J. "Universal binding energy curves for metals and bimetallic interfaces", *Physical Review Letters*, 47, pp. 675–678 (1981).
[41] Rose, J., Smith, J. and Ferrante, J. "Universal features of bonding in metals", *Physical Review B*, 28, pp. 1835–1845 (1983).
[42] Hughes, T., *The Finite Element Method. Linear Static and Dynamic Finite Element Analysi*, Dover Publications, Mineola, USA (2000).
[43] van der Merwe, R. "Sigma-point Kalman filters for probabilistic inference in dynamic state-space models", Ph.D. Thesis, Oregon Health and Science University (2004).
[44] Kalman, R.E. "A new approach to linear filtering and prediction problems", *ASME Journal of Basic Engineering*, 82D, pp. 35–45 (1960).
[45] Arulampalam, M., Maskell, S., Gordon, N. and Clapp, T. "A tutorial on particle filters for online nonlinear/non-Gaussian Bayesian tracking", *IEEE Transactions on Signal Processing*, 50, pp. 174–188 (2002).
[46] Clapp, T. "Statistical methods for the processing of communications data", Ph.D. Thesis, University of Cambridge, UK (2000).
[47] Gordon, N., Salmond, D. and Smith, A. "Novel approach to nonlinear/non-Gaussian Bayesian state estimation", *IEE Proceedings — F: Radar and Signal Processing*, 140, pp. 107–113 (1993).
[48] Julier, S. and Uhlmann, J. "A general method for approximating nonlinear transformations of probability distributions", Tech. Rep., RRG, Department of Engineering Science, University of Oxford (1996).
[49] Julier, S., Uhlmann, J. and Durrant-Whyte, H. "A new approach for filtering nonlinear systems", In *Proceedings of the American Control Conference*, 3, Seattle, pp. 1628–1632 (1995).
[50] Julier, S. "The scaled unscented transformation", In *Proceedings of the American Control Conference*, 6, Anchorage, 2002, pp. 4555–4559 (2002).
[51] Reif, K., Günther, S., Yaz, E. and Unbehauen, R. "Stochastic stability of the discrete time extended Kalman filter", *IEEE Transactions on Automatic Control*, 44, pp. 714–728 (1999).
[52] Xiong, K., Zhang, H. and Chan, C. "Performance evaluation of UKF-based nonlinear filtering", *Automatica*, 42, pp. 261–270 (2006).
[53] Crisan, D. and Doucet, A. "A survey of convergence results on particle filtering methods for practitioners", *IEEE Transactions on Signal Processing*, 50, pp. 736–746 (2002).
[54] Ljung, L. "System identification", In *Theory for the User*, 2nd edn., Prentice Hall (1999).
[55] Eftekhar Azam, S., Ghisi, A. and Mariani, S. "A parallel implementation of the sigma-point Kalman filter", In *Proceedings of CST2010, The Tenth International Conference on Computational Structures Technology*, B. Topping, J. Adam, F. Pallarés, R. Bru and M. Romero, Eds., Civil-Comp Press, Stirlingshire, Scotland, Valencia, Spain, 14–17 September (2010).
[56] Eftekhar Azam, S., Ghisi, A. and Mariani, S. "Parallelized sigma-point Kalman filtering for structural dynamics", *Computers and Structures*, 92–93, pp. 193–205 (2012).
[57] Lefebvre, T., Bruyninckx, H. and Schutter, J.D. "Kalman filters for nonlinear systems: a comparison of performance", *International Journal of Control*, 77, pp. 639–653 (2004).

Saeed Eftekhar Azam has recently obtained his Ph.D. Degree from the Department of Structural Engineering at Politecnico di Milano, Italy. He received his B.S. Degree from Tehran University and his M.S. Degree from Sharif University of Technology in Iran. His research interests include dynamics of structures, structural system identification and structural health monitoring.

Mehrdad Bagherinia is currently a Ph.D. Degree candidate at Politecnico di Milano, Italy. He received his B.S. Degree in Mechanical Engineering from Isfahan University of Technology, Iran, and his M.S. Degree in Mechanical System Design from Politecnico di Milano, in Italy. His current research activities include study and design of novel magnetic field MEMS sensors.

Stefano Mariani received an M.S. Degree (cum laude) in Civil Engineering and a Ph.D. Degree in Structural Engineering from Politecnico di Milano, Italy, in 1995 and 1999, respectively, and is currently Associate Professor in the Department of Structural Engineering at the same establishment. He is author of over 120 articles including papers published in international journals, book chapters and congress communications. He is member of the Editorial Boards of Sensors, Algorithms, Micromachines, International Journal of Information and Computer Science, and International Journal on Advances in Systems and Measurements. His research interests include numerical simulations of ductile fracture in metals and quasi-brittle fracture in heterogeneous and functionally graded materials, extended finite element methods, calibration of constitutive models via particle and Kalman filters, multi-scale solution methods for dynamic delamination in layered composites, reliability of MEMS subject to shocks and drops and structural health monitoring with MEMS.